Bis(ethylenedithio)tetrathiafulvalene (BEDT-TTF) Charge Transfer Salts of $Re_2(NCS)_{10}^{n-}$ ($n = 2, 3$)

Cameron J. Kepert,[†] Mohamedally Kurmoo,[‡] and Peter Day*

Davy Faraday Research Laboratory, The Royal Institution, 21 Albemarle Street, London W1X 4BS, U.K.

Received July 24, 1996[⊗]

Electrolytic oxidation of BEDT-TTF (bis(ethylenedithio)tetrathiafulvalene) in the presence of anionic rhenium thiocyanato complexes has led to the crystallization of two phases containing $Re_2(NCS)_{10}^{n-}$ ($n = 2, 3$), while $Re(NCS)_6^{2-}$ and $Re_2(NCS)_8^{2-}$ gave no characterizable products. (BEDT-TTF)$_3$[$Re_2(NCS)_{10}$]·2CH_2Cl_2 (**1**) and (BEDT-TTF)$_2$[$Re_2(NCS)_{10}$]·C_6H_5CN (**2**) are both triclinic ($P\bar{1}$) with unit cell parameters $a = 12.185(3)$ Å, $b = 13.251(3)$ Å, $c = 14.772(2)$ Å, $\alpha = 63.69(1)°$, $\beta = 86.56(2)°$, $\gamma = 64.50(2)°$ ($Z = 1$) and $a = 13.730(4)$ Å, $b = 14.882(4)$ Å, $c = 16.588(4)$ Å, $\alpha = 75.98(2)°$, $\beta = 85.63(2)°$, $\gamma = 66.95(2)°$ ($Z = 2$), respectively. Both salts present packing arrangements of BEDT-TTF not found before. In compound **1** mixed layers of anions and cations contain no stacks of BEDT-TTF. In **2** there are layers of segregated anions and cations, the latter having their long axes nearly parallel to the layers. This compound is the first in which $Re_2(NCS)_{10}^{2-}$ has been structurally characterized. In both compounds there are numerous close S−S contacts between the NCS ligands and the BEDT-TTF. The compounds are semiconductors, the conductivity being attributed to low-dimensional hopping rather than coherent transport. The magnetic properties of **1** are modeled by a superposition of a Curie−Weiss contribution for the anion and a dimer contribution from the cation.

Charge transfer salts of BEDT-TTF (bis(ethylenedithio)-tetrathiafulvalene) have captured wide attention because of the remarkable variety both of crystal structures and physical properties that they exhibit.[1] Among the latter are semiconductivity, superconductivity, charge density waves, spin density waves, and spin−Peierls transitions, that is, properties associated with a low-dimensional electronic structure. Low dimensionality comes about because the BEDT-TTF cations and inorganic anions are segregated into well-defined alternating layers in the vast majority of structures determined so far. The electronic states closest to the Fermi surface are those of the organic donor, and no examples exist until now in which electronic states of the anions contribute significantly to the conductivity. Indeed, where paramagnetic states are associated with the anions, it has been found that they scarcely interact at all with the electronic states of the organic sublattice, which can be metallic or even superconducting. In an effort to increase interaction between the anion and cation sublattices in this class of compounds and hence influence the electronic dimensionality, we have taken two approaches. First, one might hope to vary the band filling of the cation sublattice by making salts containing anions whose charge can easily be varied either by redox processes or by protonation. An example of the latter is the use of HPO_2^- and $H_2PO_4^-$ in attempting the synthesis of solid solutions,[2] while transition metal complexes have the potential for multiple oxidation states. A second way to increase interaction between the two sublattices is to make salts with anions that have the potential to bond with the S atoms on the cations. Given that S···S interactions are common in this class of compounds, anionic thiocyanato complexes in which the N is bonded to a transition metal are attractive targets, especially where multiple oxidation states are found.

While no BEDT-TTF salts containing uncomplexed thiocyanate are known, several containing anionic thiocyanate complexes have been reported. These include the 10 K superconductor κ-(BEDT-TTF)$_2$[$Cu(NCS)_2$],[3] the superconducting/metallic series (BEDT-TTF)$_2$X[$Hg(SCN)_4$] (X = NH_4^+, Na^+, K^+, Rb^+, Cs^+, Tl^+),[4] and a metallic series of the form α-(BEDT-TTF)$_2$X[$M(NCS)_4$] (X = K^+, Rb^+, Cs^+; M = Co^{2+}, Zn^{2+}, Cd^{2+}).[5] In all cases except the 10 K superconductor the S is bonded to the metal and hence not available for interaction with the BEDT-TTF. In the present paper we report two BEDT-TTF salts of $Re_2(NCS)_{10}^{n-}$ ($n = 2, 3$) in both of which significant interaction is seen between the S of the thiocyanate and BEDT-TTF, sufficient enough to disrupt the conventional layer packing. Both compounds contain stacking arrangements of BEDT-TTF of a type not observed before.

Experimental Section

Syntheses. ($N(n\text{-}Bu)_4)_2$[$Re_2(NCS)_8$] was prepared following the method of Cotton *et al.*,[6] by the reaction of ($N(n\text{-}Bu)_4)_2$[Re_2Cl_8] (0.91 g) and NaSCN (0.60 g) in acidified methanol. Recrystallization from dichloromethane and diethyl ether produced deep red plates.

($N(n\text{-}Bu)_4)_2$[$Re(NCS)_6$] and ($N(n\text{-}Bu)_4)_3$[$Re_2(NCS)_{10}$] were prepared following the method of Cotton *et al.*,[6] by the reaction of ($N(n\text{-}Bu)_4)_2$-[Re_2Cl_8] (1.58 g) and NaSCN (1.23 g) in acetone over 4 h.

Crystal growth was carried out electrochemically in conventional H-shaped cells using tetra-*n*-butylammonium salts of the anionic Re complexes as the supporting electrolyte. Using ($N(n\text{-}Bu)_4)_2$[$Re(NCS)_6$] in CH_2Cl_2 with a current of 0.5 μA, very fine, black needles formed

[†] Present address: Inorganic Chemistry Laboratory, South Parks Road, Oxford OX1 3QR, U.K.

[‡] Present address: IPCMS-GMI, 23 Rue Loess, B. P. 20/CR, 67037 Strasbourg Cedex, France.

[⊗] Abstract published in *Advance ACS Abstracts,* February 15, 1997.

(1) Williams, J. M.; Ferraro, J. R.; Thorn, R. J.; Carlson, K. D.; Geiser, U.; Wang, H. H.; Kini, A. M; Whangbo, M.-H. *Organic Superconductors (Including Fullerenes): Synthesis, Structure, Properties and Theory*; Prentice Hall: Englewood Cliffs, NJ, 1992.

(2) Kurmoo, M.; Kanazawa, D.; Day, P. *Synth. Met.* **1991**, *91*−*93*, 2123.

(3) Urayama, H.; Yamochi, H.; Saito, G.; Sato, S.; Kawamoto, A.; Tanaka, J.; Mori, T.; Maruyama, Y; Inokuchi, H. *Chem. Lett.* **1988**, 463.

(4) Oshima, M.; Mori, H.; Saito, G.; Oshima, K. *Chem. Lett.* **1989**, 1159.

(5) Mori, H.; Hirabayashi, I.; Tanaka, S.; Mori, T; Maruyama, Y. *Synth. Met.* **1995**, *70*, 789.

(6) Cotton, F. A.; Robinson, W. R.; Walton, R. A.; Whyman, R. *Inorg. Chem.* **1967**, *6*, 929.

S0020-1669(96)00884-1 CCC: $14.00

Table 1. Crystal and Refinement Data for $(BEDT\text{-}TTF)_3[Re_2(NCS)_{10}]\cdot 2CH_2Cl_2$ and $(BEDT\text{-}TTF)_2[Re_2(NCS)_{10}]\cdot C_6H_5CN$[a]

	$(BEDT\text{-}TTF)_3[Re_2(NCS)_{10}]\cdot 2CH_2Cl_2$	$(BEDT\text{-}TTF)_2[Re_2(NCS)_{10}]\cdot C_6H_5CN$
chem formula	$C_{42}H_{28}Cl_4N_{10}Re_2S_{34}$	$C_{37}H_{21}N_{11}Re_2S_{26}$
a/Å	12.185(3)	13.730(4)
b/Å	13.251(3)	14.882(4)
c/Å	14.772(2)	16.588(4)
α/deg	63.69(1)	75.98(2)
β/deg	86.56(2)	85.63(2)
γ/deg	64.50(2)	66.95(2)
V/Å^3	1904.0(7)	3025(2)
Z	1	2
M/(g mol^{-1})	2277.0	1825.6
space group	$P\bar{1}$	$P\bar{1}$
T/°C	295	295
λ/Å	0.710 69	0.710 69
ρ_{calcd}/(g cm^{-3})	1.99	2.00
μ(Mo-K$_\alpha$)/cm^{-1}	42.3	49.6
$R(F_o)$/% (all data)	5.28 (6.33)	5.08 (7.30)
$R_w(F_o)$/%	4.97	5.03

[a] $R(F_o) = \sum_s||F_o(S)| - |F_c(S)||/\sum_s|F_o(S)|$ and $R_w(F_o) = \sum_s(w(S))^{1/2}||F_o(S) - |F_c(S)||)/\sum_s(w(S))^{1/2}|F_o(S)|)$.

on the anode in one experiment, while in another thin, black plates formed, unsuitable for crystallography. In benzonitrile at a current of 0.5 μA, the same salt gave only a thin, black, polycrystalline coating on the anode over a period of several weeks. The cell was subsequently connected to a constant voltage source of 5 V in an attempt to produce $(BEDT\text{-}TTF)_2^{2+}$ but no further precipitation occurred.

With $(N(n\text{-}Bu)_4)_2[Re_2(NCS)_8]$ as electrolyte in dichloromethane no precipitation occurred at a current of 0.5 μA or increasing to 2.0 μA, while in benzonitrile at a current of 0.5 μA, only a black, amorphous coating formed on the anode. In contrast $(N(n\text{-}Bu)_4)_3[Re_2(NCS)_{10}]$ in CH_2Cl_2 at a current of 0.5 μA yielded large, high-quality, black, hexagonal plates of $(BEDT\text{-}TTF)_2[Re_2(NCS)_{10}]\cdot 2CH_2Cl_2$, while in benzonitrile at the same current, high-quality blocklike crystals of $(BEDT\text{-}TTF)_2[Re_2(NCS)_{10}]\cdot C_6H_5CN$ formed on the anode.

Crystal Structure Determination. Room temperature X-ray data collections were made on a Nicolet R3mV four-circle diffractometer equipped with a graphite monochromatized Mo Kα radiation source ($\lambda = 0.71073$ Å). Crystals were mounted in beryllium glass capillaries. Complete hemispheres of data were recorded using $\omega-2\theta$ scans in the range $5° < 2\theta < 50°$. Three standard reflections were measured every 97 reflections to monitor crystal deterioration and X-ray beam intensity. For the purpose of empirical absorption correction ψ-scan collections with 10° increments were performed on 10 peaks. The structures were solved using Patterson methods and refined using full matrix least-squares optimization (SHELXTL PLUS).

$(BEDT\text{-}TTF)_3[Re_2(NCS)_{10}]\cdot 2CH_2Cl_2$. The unit cell was refined from 23 reflections ($17.2° < 2\theta < 27.2°$). Consideration of the crystal orientation matrix and the polarized infrared reflectivity spectra suggested an index of {201} for the large crystal face. However, both analytical and empirical laminar absorption corrections with this and a variety of other indices gave inferior results to an empirical ellipsoidal correction. Further details of the data collection, processing, and structural refinement are given in Table 1, and as Supporting Information.

The structural refinement was complicated by random disorder. The 50% occupation of the $(BEDT\text{-}TTF)_B\cdot CH_2Cl_2$ unit about the $(0,0,^1/_2)$ inversion center is a source of strong correlation, due to the near-equivalence of many inversion-related atomic positions. Hence, care was taken to model the atomic and thermal parameters avoiding highly correlated parameters. All $(BEDT\text{-}TTF)_B$ sulfur atoms were refined anisotropically except for S(22), S(24), and S(25) which approximately superimpose onto the inversion-related positions of C(25), C(29), and Cl(2), respectively. S(22) and S(24) were given fixed temperature factors equal to the isotropic equivalent of atoms S(21) and S(23), while the temperature factor of S(25) was refined. Carbon atoms of $(BEDT\text{-}TTF)_B$ were refined isotropically. The position of C(29) was fixed to the site located in the difference map. The CH_2Cl_2 molecule was refined isotropically. No hydrogen atoms were added to the $(BEDT\text{-}TTF)_B\cdot CH_2Cl_2$ unit.

The disorder present in one ethylene group of molecule A and in the second CH_2Cl_2 was treated by fixing isotropic thermal parameters and refining atomic occupations. The CH_2Cl_2 molecule was found in multiple orientations about the $(^1/_2,0,0)$ inversion center. Three distinct Cl atom positions were found equidistant from the inversion center, and their occupation was refined. Carbon atom coordinates were found from the Fourier difference map corresponding to the 55% occupied CH_2Cl_2 orientation.

Tables of atomic coordinates, equivalent isotropic displacement parameters, site occupation factors, and anisotropic displacement paramenters are available as Supporting Information. Selected intramolecular bond lengths and angles are listed in Table 2 and the shortest intermolecular S—S distances in Table 3. The atomic numbering scheme and thermal ellipsoids are shown in Figure 1.

$(BEDT\text{-}TTF)_2[Re_2(NCS)_{10}]\cdot C_6H_5CN$. The unit cell was determined and refined from 25 reflections ($21.0° < 2\theta < 27.8°$). Analytical absorption correction gave inferior results to the ellipsoid empirical correction, with merging *R*-factors of 6.32, 3.04, and 2.36% for the raw, analytically-corrected and empirically-corrected data sets, respectively. Details of the data collection, processing, and structural refinement are in Table 1, and as Supporting Information.

The small degree of disorder in the bridging NCS of $[Re_2(NCS)_{10}]^{2-}$ was treated by refining positional and occupational parameters of two further terminal sulfur atom sites. Tables of atomic coordinates, equivalent isotropic displacement parameters, site occupation factors, and anisotropic displacement parameters are available as Supporting Information. Selected intramolecular bond lengths and angles are listed in Table 4 and the shortest intermolecular S—S distances in Table 5.

Table 2. Selected Intramolecular Bond Lengths (Å) and Angles (deg) of $(BEDT\text{-}TTF)_3[Re_2(NCS)_{10}]\cdot 2CH_2Cl_2$

Re(1)−Re(1A)	2.602 (1)	S(13)−C(12)	1.699(9)
Re(1)−N(1)	2.091(8)	S(13)−C(15)	1.724(10)
Re(1)−N(1A)	2.069(8)	S(14)−C(12)	1.716(10)
Re(1)−N(2)	2.017(8)	S(14)−C(16)	1.727(8)
Re(1)−N(3)	2.043(8)	S(21)−C(21)	1.715(31)
Re(1)−N(4)	2.010(7)	S(21)−C(23)	1.726(16)
Re(1)−N(5)	1.988(8)	S(22)−C(21)	1.684(26)
N(1)−C(1)	1.176(17)	S(22)−C(24)	1.731(19)
N(2)−C(2)	1.174(14)	S(23)−C(22)	1.727(20)
N(3)−C(3)	1.155(13)	S(23)−C(25)	1.641(18)
N(4)−C(4)	1.161(11)	S(24)−C(22)	1.721(25)
N(5)−C(5)	1.167(13)	S(24)−C(26)	1.790(17)
S(1)−C(1)	1.561(14)	C(11)−C(12)	1.382(10)
S(2)−C(2)	1.606(12)	C(13)−C(14)	1.369(14)
S(3)−C(3)	1.601(11)	C(15)−C(16)	1.374(16)
S(4)−C(4)	1.618(9)	C(21)−C(22)	1.383(26)
S(5)−C(5)	1.606(11)	C(23)−C(24)	1.331(33)
S(11)−C(11)	1.722(10)	C(25)−C(26)	1.415(36)
S(11)−C(13)	1.737(7)	C(31)−Cl(1A)	1.66(4)
S(12)−C(11)	1.720(8)	C(32)−Cl(2)	1.74(5)
S(12)−C(14)	1.739(9)	C(32)−Cl(3)	1.61(8)
N(1)−Re(1)−N(1A)		102.6 (3)	
Cl(1A)−C(31)−Cl(1A)*		124(2)	
Cl(2)−C(32)−Cl(3)		116(4)	

Table 3. Shortest Intermolecular Sulfur−Sulfur Distances (Å) in $(BEDT\text{-}TTF)_3[Re_2(NCS)_{10}]\cdot 2CH_2Cl_2$[a]

molecule	inner−inner	inner−outer	outer−outer
A−A	4.01	3.82	3.82
A−B	3.73	3.38	3.78
B−B	>4.0	3.93	4.00

molecule	inner	inner−outer	outer
A−anion	3.22		3.64
B−anion	3.44		3.46
anion−anion		3.66	

[a] "Inner" and "outer" denote S atoms of the TTF and bis(ethylenedithio) moieties, respectively.

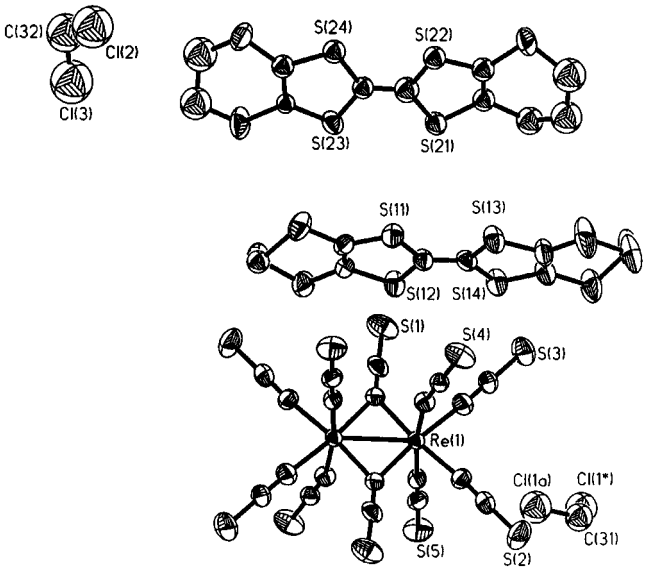

Figure 1. Atomic numbering scheme of $(BEDT\text{-}TTF)_3[Re_2(NCS)_{10}]\cdot 2CH_2Cl_2$ (showing 50% anisotropic thermal ellipsoids).

Table 4. Selected Intramolecular Bond Lengths (Å) and Angles (deg) of $(BEDT\text{-}TTF)_2[Re_2(NCS)_{10}]\cdot C_6H_5CN$

Re(1)−Re(2)	2.615(1)	C(9)−S(9)	1.569(12)
Re(1)−N(1)	2.058(9)	C(10)−S(10)	1.577(10)
Re(1)−N(2)	2.045(7)	S(11)−C(11)	1.716(10)
Re(1)−N(3)	2.001(10)	S(11)−C(13)	1.714(12)
Re(1)−N(4)	1.975(11)	S(12)−C(11)	1.726(12)
Re(1)−N(5)	2.013(8)	S(12)−C(14)	1.736(10)
Re(1)−N(6)	2.010(9)	S(13)−C(12)	1.720(13)
Re(2)−N(1)	2.076(7)	S(13)−C(15)	1.748(10)
Re(2)−N(2)	2.070(8)	S(14)−C(12)	1.714(11)
Re(2)−N(7)	1.975(10)	S(14)−C(16)	1.736(12)
Re(2)−N(8)	2.010(10)	S(21)−C(21)	1.735(12)
Re(2)−N(9)	2.013(9)	S(21)−C(23)	1.740(12)
Re(2)−N(10)	2.035(8)	S(22)−C(21)	1.706(13)
N(1)−C(1)	1.200(13)	S(22)−C(24)	1.749(10)
N(2)−C(2)	1.182(12)	S(23)−C(22)	1.717(14)
N(3)−C(3)	1.180(15)	S(23)−C(25)	1.756(10)
N(4)−C(4)	1.190(17)	S(24)−C(22)	1.734(12)
N(5)−C(5)	1.174(12)	S(24)−C(26)	1.704(12)
N(6)−C(6)	1.145(15)	C(11)−C(12)	1.377(13)
N(7)−C(7)	1.163(17)	C(13)−C(14)	1.370(18)
N(8)−C(8)	1.166(15)	C(15)−C(16)	1.362(19)
N(9)−C(9)	1.162(15)	C(21)−C(22)	1.361(14)
N(10)−C(10)	1.157(12)	C(23)−C(24)	1.357(18)
N(31)−C(31)	1.131(23)	C(25)−C(26)	1.343(19)
C(1)−S(1)	1.535(11)	C(31)−C(32)	1.445(21)
C(2)−S(2)	1.566(10)	C(32)−C(33)	1.379(23)
C(3)−S(3)	1.581(13)	C(32)−C(37)	1.416(17)
C(4)−S(4)	1.555(14)	C(33)−C(34)	1.350(21)
C(5)−S(5)	1.579(10)	C(34)−C(35)	1.380(19)
C(6)−S(6)	1.615(13)	C(35)−C(36)	1.335(22)
C(7)−S(7)	1.592(15)	C(36)−C(37)	1.356(20)
C(8)−S(8)	1.596(12)		

N(1)−Re(1)−N(2)	102.0(3)
N(1)−Re(2)−N(2)	100.6(3)

The asymmetric unit with atom numbering and thermal ellipsoids are shown in Figure 2.

Physical Measurements. Because of the small size of the crystals, only two-probe dc electrical conductivity measurements were made from 300 to 130 K. Gold wire electrodes (25 μm) were attached directly to single crystals using platinum paint. However, because the resistance of the crystals is high, contact resistance is not expected to be important.

Magnetic susceptibility and magnetization measurements were made on polycrystalline samples of $(BEDT\text{-}TTF)_3[Re_2(NCS)_{10}]\cdot 2CH_2Cl_2$ using a Quantum Design MPMS 7 SQUID magnetometer. The sample was placed inside a gelatin capsule in a plastic tube. The susceptibility was measured from 4 to 250 K in a field of 1 T and the magnetization from 0 to 7 T at 5 K.

Table 5. Shortest Intermolecular Sulfur−Sulfur Distances (Å) in $(BEDT\text{-}TTF)_2[Re_2(NCS)_{10}]\cdot C_6H_5CN$[a]

molecule	inner−inner	inner−outer	outer−outer
A−A	3.63	3.61	3.88
A−B	3.99	3.67	3.54
B−B	3.68	3.77	3.98

molecule	inner	outer
A−anion	3.31	3.56
B−anion	3.44	3.43
anion−anion	3.57	

[a] "Inner" and "outer" denote S atoms of the TTF and bis(ethylenedithio) moieties, respectively.

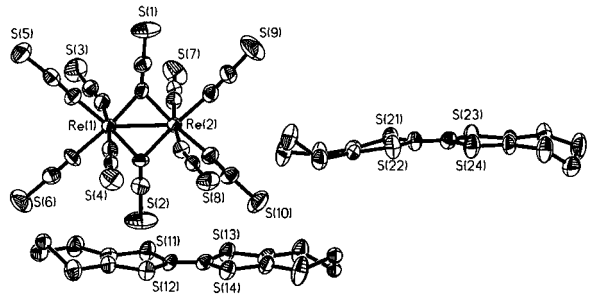

Figure 2. Atomic numbering scheme of $(BEDT\text{-}TTF)_2[Re_2(NCS)_{10}]\cdot C_6H_5CN$ (showing 50% anisotropic thermal ellipsoids). The C_6H_5CN molecule is omitted for clarity.

Infrared reflectivity of single crystals was measured at room temperature using a Perkin-Elmer 1710 Fourier transform spectrometer equipped with a microscope attachment.

Results and Discussion

Syntheses. The fact that only very poor crystals resulted for electrooxidation of BEDT-TTF in the presence either of $[Re(NCS)_6]^{2-}$ or $[Re_2(NCS)_8]^{2-}$ suggests that these spiderlike anions have shapes and charges that are unsuited to the efficient packing with $(BEDT\text{-}TTF)^{n+}$. In contrast, electrooxidation of BEDT-TTF in the presence of $[Re_2(NCS)_{10}]^{n-}$ ($n = 2, 3$) readily gave high-quality crystals. When intermolecular orbital overlap is insufficient to allow significant electron delocalization, the charges on the molecular cations are constrained to integral values; hence, balancing the charge-to-size ratio is important in producing efficient molecular packing in the crystal.

Crystal Structures. The structural refinement of $(BEDT\text{-}TTF)_3[Re_2(NCS)_{10}]\cdot 2CH_2Cl_2$ reveals much inherent local disorder, though the sharpness of the X-ray reflections indicates long-range crystalline order. Intensity statistics strongly suggest centrosymmetric symmetry, and the triclinic space group $P\bar{1}$. Extended exposure Weissenberg photographs were free of satellite reflections and diffuse features, indicating true random occupation without significant correlation between neighboring cells. The asymmetric unit contains half of the $[Re_2(NCS)_{10}]^{3-}$ (centered on the $(0,{}^1/_2,0)$ inversion center); one BEDT-TTF on a general position ($BEDT\text{-}TTF_A$); one CH_2Cl_2 molecule heavily disordered about the $({}^1/_2,0,0)$ inversion center; and a hydrogen-bonded $(BEDT\text{-}TTF)_B\cdot CH_2Cl_2$ unit, randomly disordered with 50% occupation about the $(0,0,{}^1/_2)$ inversion center. The CH_2Cl_2 Cl atoms H-bond to the ethylene group H atoms of $(BEDT\text{-}TTF)_B$. Atom Cl(2) forms a single H-bond to H(30B) with a distance of 2.97 Å, while atom Cl(3) bonds to both H(29B) and H(30B) with distances of 3.24 and 3.34 Å, respectively. Although disorder in the BEDT-TTF ethylene groups and incorporated solvent molecules is common in BEDT-TTF salts, the partial occupation of a BEDT-TTF molecule on a discrete site has never been reported before.

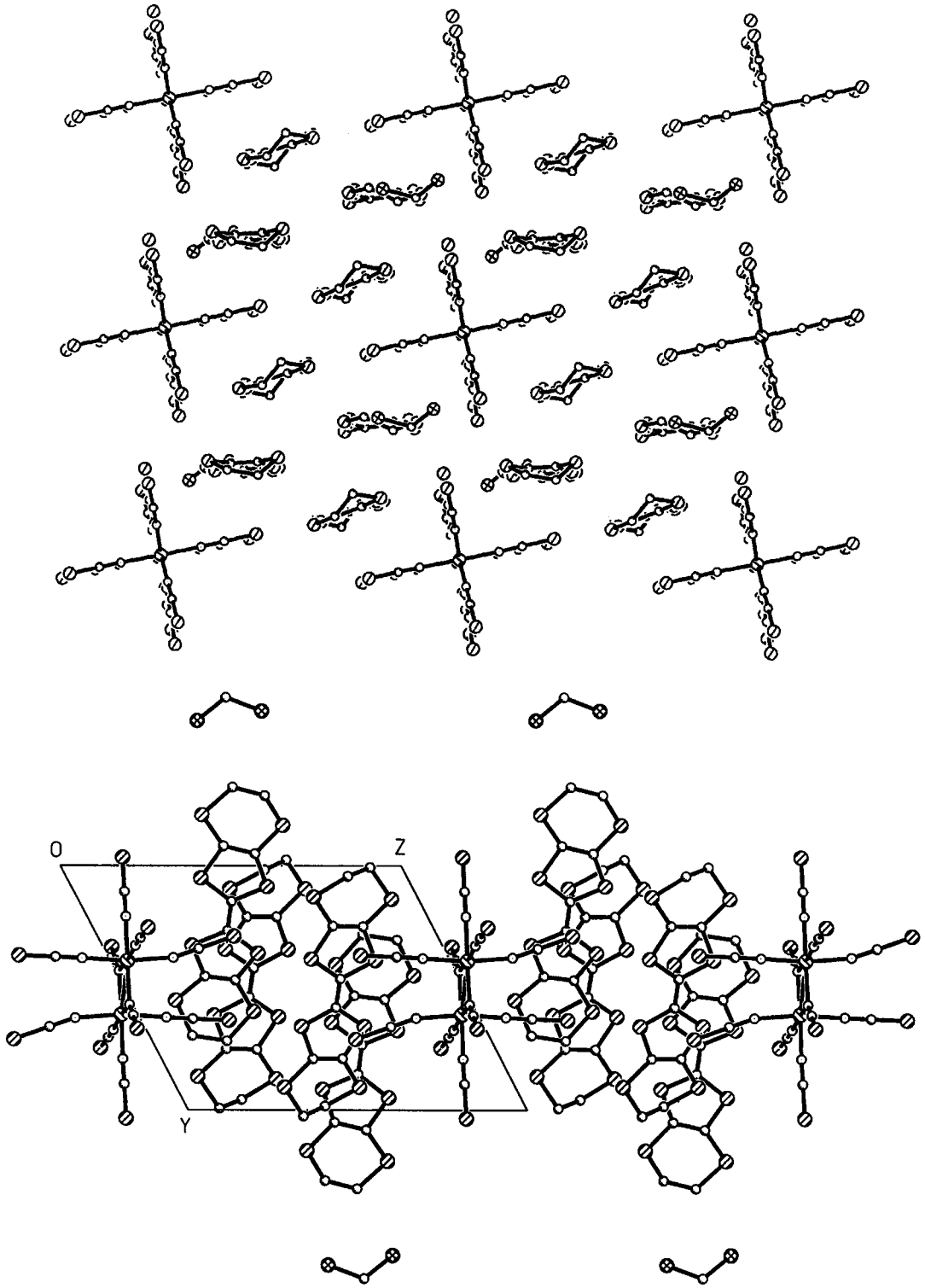

Figure 3. Projection of the structure $(BEDT\text{-}TTF)_3[Re_2(NCS)_{10}]\cdot 2CH_2Cl_2$: (a, top) down the BEDT-TTF long axes; (b, bottom) down the *a*-axis (for simplicity only one orientation of the disordered $ET_B\cdot CH_2Cl_2$ unit is shown).

The structure represents an entirely new packing phase mode among BEDT-TTF salts, in which there is no continuous network of closely-interacting BEDT-TTF. Such a feature naturally raises questions about the importance of long-range intermolecular interactions between the cations. However, several very short intermolecular S−S distances between cations and the anion (Table 3) constitute a continuous 3-D network, never seen before in BEDT-TTF salts.

Roughly speaking the structure may be viewed as consisting of layers in the *ac*-plane that contain both cations and anions (Figure 3a,b). This description is complicated by the presence of disorder in the $BEDT\text{-}TTF_B\cdot CH_2Cl_2$ unit, which, if centered on the $y = n$ inversion center, may be oriented so that the $BEDT\text{-}TTF_B$ molecule lies either within the $y = n - {}^1/_2$ or the $y = n + {}^1/_2$ layer. For simplicity Figure 3b shows all four $BEDT\text{-}TTF_B$ molecules oriented at $y \sim {}^1/_2$.

The intramolecular C−S and C═C bond lengths of the ordered molecule A suggest a charge of +1. Despite the disorder of B, the bond lengths in the central part of the molecule are sufficiently well-defined to indicate that the charge is likewise +1. The ethylene groups in both BEDT-TTF molecules adopt the chair conformation. Refinement of the disorder

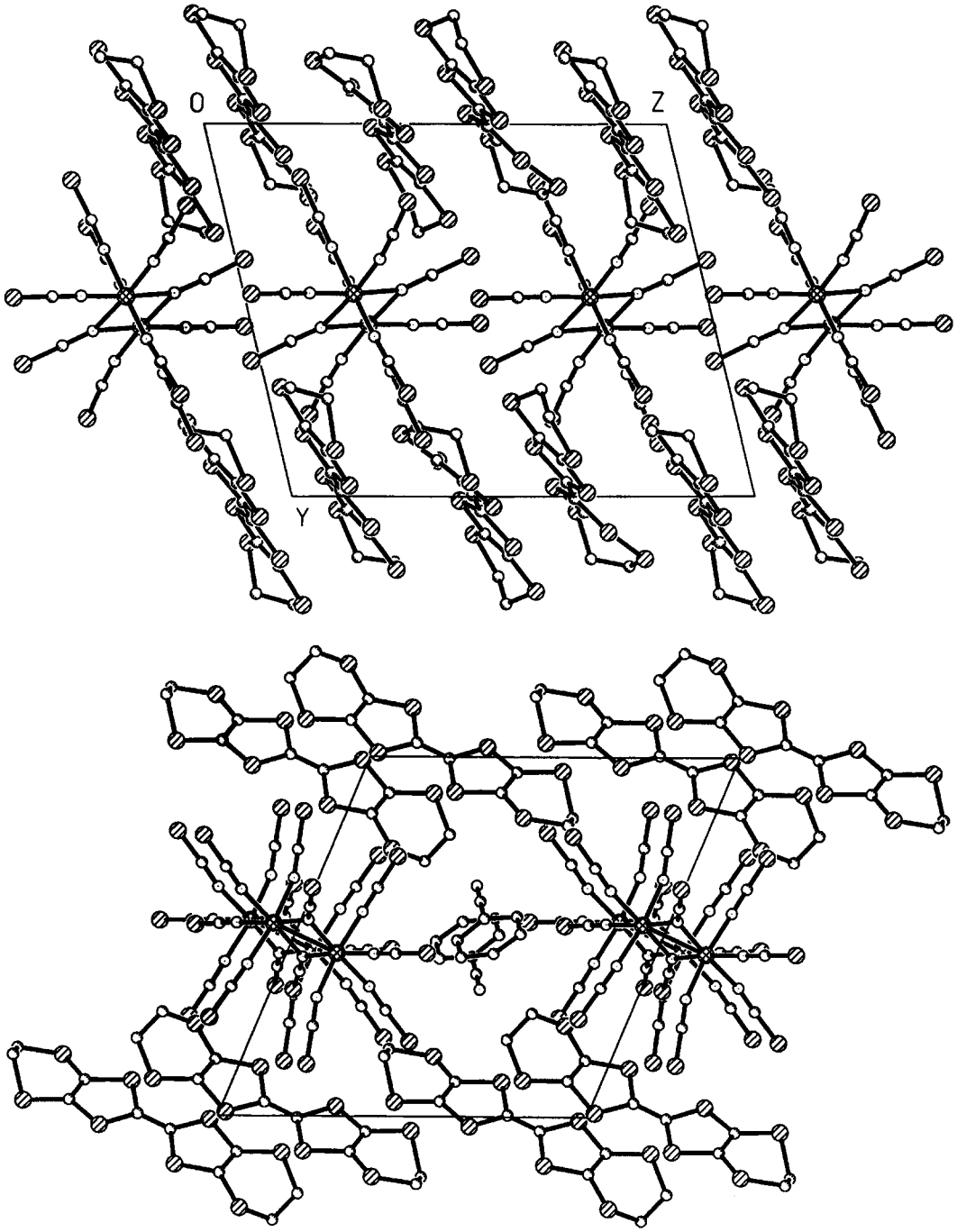

Figure 4. Projection of $(BEDT\text{-}TTF)_2[Re_2(NCS)_{10}]\cdot C_6H_5CN$: (a, top) down the *a*-axis (the C_6H_5CN molecule is omitted for clarity); (b, bottom) down the *c*-axis.

of C(17) (molecule A) indicates that about 75% of these molecules are in the eclipsed conformation and 25% staggered. The ethylene groups of molecule B are ordered in the eclipsed conformation.

$(BEDT\text{-}TTF)_2[Re_2(NCS)_{10}]\cdot C_6H_5CN$ crystallizes in the triclinic space group $P\bar{1}$, with an asymmetric unit containing one $[Re_2(NCS)_{10}]^{2-}$ anion, two BEDT-TTF cations, and one C_6H_5CN. All are in general positions. In contrast to the packing arrangement found in $(BEDT\text{-}TTF)_3[Re_2(NCS)_{10}]\cdot 2CH_2Cl_2$, the structure of $(BEDT\text{-}TTF)_2[Re_2(NCS)_{10}]\cdot C_6H_5CN$ consists of discrete cationic and anionic layers. These lie in the *ac*-plane and are shown side-on in projections down the *a*- and *c*-axes in Figure 4 and front-on in projections down the *b*-axis in Figure 5. The packing of the BEDT-TTF layer is very unusual, with the long axes of the molecules almost parallel to the layer. The axes of molecules A and B make angles to the layer of 27.7 and 25.2°, respectively, giving a perpendicular cross-sectional area of 25.3 Å^2/molecule. Since the area occupied by the anions in the *ac*-plane is large enough to accommodate at least twice as many BEDT-TTF molecules in a more vertical orientation, it is likely that the packing arrangement arises, not from the mismatch of cation and anion layer periodicities, but from the S—S interactions between layers. As in $(BEDT\text{-}TTF)_3[Re_2(NCS)_{10}]\cdot 2CH_2Cl_2$, there is no continuous network of short intermolecular S—S contacts between neighboring BEDT-TTF molecules. Indeed, for any interaction, there are at most two such S—S distances shorter than 4 Å (Table 5). However, there are several very short S—S contacts between the cations and anions, forming a continuous network through the structure.

The intramolecular bond lengths C—S and C═C of the two discrete BEDT-TTF indicate that each cation has a charge close to +1. Both ethylene groups of molecule A are disordered,

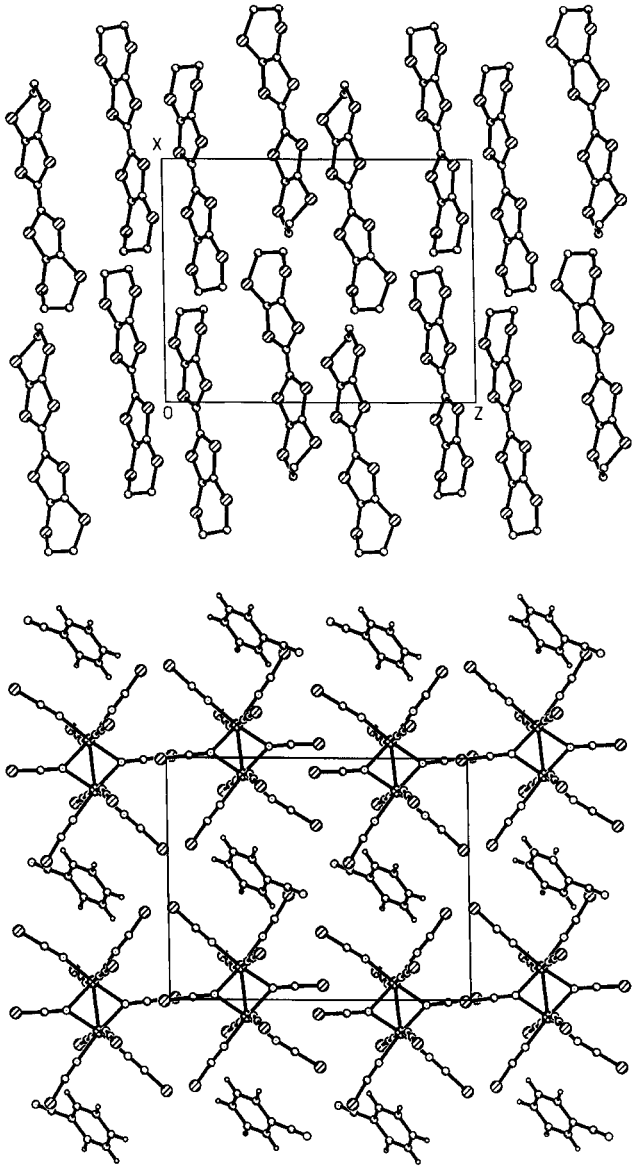

Figure 5. Projection of the cation (a, top) and anion (b, bottom) layers of (BEDT-TTF)$_2$[Re$_2$(NCS)$_{10}$]·C$_6$H$_5$CN down the *b*-axis.

while molecule B is fully ordered and exhibits the staggered conformation. It is worth emphasizing that this salt represents the first instance in which $[Re_2(NCS)_{10}]^{n-}$ has been structurally characterized in the dinegative state. We are therefore in a position to compare the geometry of $[Re_2(NCS)_{10}]^{2-}$ with that of $[Re_2(NCS)_{10}]^{3-}$.

A recent solution electrochemistry infrared spectroscopic study has shown that $[Re_2(NCS)_{10}]^{n-}$ anions are stable for charges $n = 2$, 3, and 4, although they decompose irreversibly outside this range.[7] The structure of the trinegative anion has been previously reported in $(N(n\text{-}Bu)_4)_3[Re_2(NCS)_{10}]$.[8] In the latter the edge-shared bioctahedral (ESBO) structure is compressed along the Re—Re axis (with a N—Re—N angle to the bridging NCS of 102°), indicating bond formation between the two Re centers. The trinegative anion has been reported as of valence equalized (class III) mixed-valence type, although the observation of two ν(CN) modes for the bridging ligands suggests there is localization on the time scale of molecular vibrations.

According to the simple molecular orbital (MO) bonding scheme for the ESBO, six orbitals, with energies given by $\sigma < \pi < \delta < \delta^* < \pi^* < \sigma^*$, are formed.[9] Theoretical studies have shown, however, that reversal of the closely spaced δ and δ^* molecular orbitals may occur if the ligands are of suitable symmetry so as to interact with the metal d-orbitals.[10] Under such a scheme the formal Re—Re bond order of $[Re_2(NCS)_{10}]^{n-}$ would decrease rather than increase with increasing oxidation. However, the effect on the Re—Re bond distance may be small, because the δ-bond does not contribute strongly to the total Re—Re bond energy. Furthermore, increasing electrostatic repulsion between the metal ions with increasing oxidation state should also lead to a lengthening of the Re—Re distance. In fact, in the present work the Re—Re distance increases from 2.602(1) Å in the $n = 3$ anion to 2.615(1) Å in the $n = 2$ case, consistent with the increase in electrostatic repulsion, and potentially also to the reversal of the δ and δ^* orbitals. However, the Re—Re distance previously reported[9] of 2.613(1) Å for the trinegative anion differs significantly from that found in the BEDT-TTF salt, suggesting that the crystalline environment may influence the anion geometry. As far as other bond lengths are concerned, in general the C—S distances decrease with increasing oxidation, while Re—N and N—C distances remain unchanged within the large spread of the data (Tables 2 and 4). In the $n = 3$ anion, it may be significant that the S—C distance of the bridging NCS is shorter than those of the terminal ones.

Electrical Conductivity. Two-probe dc transport measurements on (BEDT-TTF)$_3$[Re$_2$(NCS)$_{10}$]·2CH$_2$Cl$_2$ parallel and perpendicular to the crystal plates reveal semiconducting behavior, from 130 to 300 K with room temperature conductivities σ_{RT}(along plate) $\sim$ 0.01 S cm^{-1} and σ_{RT}(through plate) $\sim$ 0.0005 S cm^{-1}. There is a slight temperature dependence of the activation energy, which varies smoothly from 0.19 eV at 300 K to 0.15 eV at 130 K. The electronic hopping model,[11] for which $\sigma \propto \exp(1/T^{(d+1)})$, fits the data closely, compared with the Boltzmann law $\sigma \propto \exp(1/T)$ (Figure 6), and yields values for the dimensionality *d* of 1.3 and 1.2 respectively parallel and perpendicular to the crystal plate. It is not clear what role the anion plays in the hopping mechanism, although it seems probable that overlap between π-orbitals of the anion and the HOMO of the BEDT-TTF moderate the tunneling barrier.

Two-probe dc transport measurement on (BEDT-TTF)$_2$[Re$_2$(NCS)$_{10}$]·C$_6$H$_5$CN perpendicular to the crystal plates shows that it is also semiconducting, likewise with a temperature-dependent activation energy, varying smoothly from 0.18 eV at 170 K to 0.26 eV at 300 K. The room temperature conductivity is $\sim$0.001 S cm^{-1}. In this compound, too, the conductivity is described very well by the hopping model (Figure 6b). It should be noted that the decreasing activation energy in both compounds with increasing temperature is inconsistent with coherent semiconducting transport. Nevertheless, while neither compound contains a continuous network of strongly interacting BEDT-TTF molecules, we find significant electrical conduction in both cases.

Magnetic Susceptibility. No magnetic properties of compounds containing $[Re_2(NCS)_{10}]^{n-}$ anions ($n = 2-4$) have been reported before. If the molecular orbital picture is upheld, the

(7) Best, S. P.; Clark, R. J. H.; Humphrey, D. G. *Inorg. Chem.* **1979**, *34*, 1013.
(8) Cotton, F. A.; Davidson, A.; Ilsley, W. H; Trop, H. S. *Inorg. Chem.* **1979**, *18*, 2719.
(9) Cotton, F. A.; Walton, R. A. *Multiple Bonds Between Metal Atoms*, 2nd ed.; Clarendon Press: Oxford, U.K., 1993.
(10) Shaik, S.; Hoffman, R.; Fisel, C. R.; Summerville, R. H. *J. Am. Chem. Soc.* **1980**, *102*, 4555.
(11) Mott, N. F. *Philos. Mag.* **1969**, *19*, 835. Zuppiroli, L. In *Low-Dimensional Conductors and Semiconductors*; Jérome, D., Caron, L. G., Eds.; NATO ASI Series BISS, Plenum Press: London, 1987; p 307.

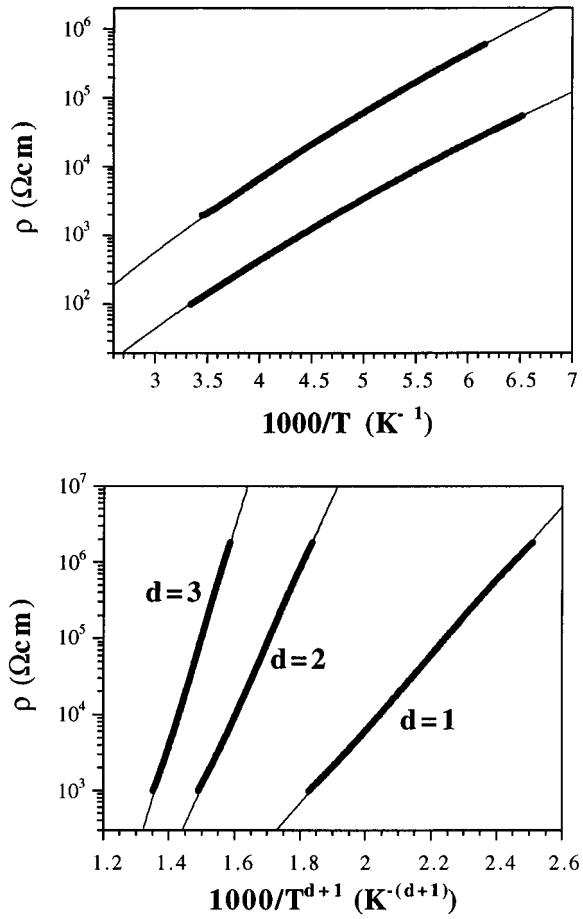

Figure 6. (a, top) 1-D hopping modeling of the electrical transport of $(BEDT\text{-}TTF)_3[Re_2(NCS)_{10}]\cdot 2CH_2Cl_2$. (b, bottom) Electrical transport of $(BEDT\text{-}TTF)_2[Re_2(NCS)_{10}]\cdot C_6H_5CN$.

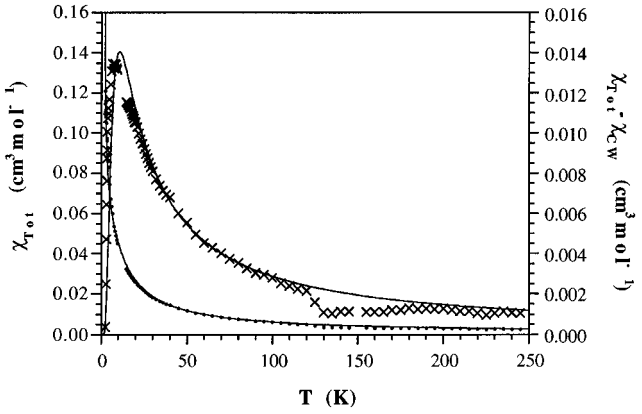

Figure 7. Total susceptibility (filled circles) and modeled residual susceptibility (crosses) of $(BEDT\text{-}TTF)_3[Re_2(NCS)_{10}]\cdot 2CH_2Cl_2$ fitted to the sum of Curie−Weiss and dimer contributions.

evenly-charged species are expected to be diamagnetic, whereas the trinegative anion is expected to behave as a $S = {}^1/_2$ Curie−Weiss paramagnet.

The variation of the product χT of $[Re_2(NCS)_{10}]\cdot 2CH_2Cl_2$ with temperature indicates that the magnetization approximately doubles between 4 and 300 K. The total susceptibility is best modeled as the sum of Curie−Weiss ($C = 0.30$ (emu K)/mol, $\Theta = 0$ K) and dimer ($J = 8.5$ K, one $S = {}^1/_2$ spin per unit cell, $n = 80\%$) contributions (Figure 7). The fit was significantly inferior when the data were modeled as the sum of Curie−Weiss and uniform antiferromagnetic chain (Bonner−Fisher) contributions. No reliable refinement could be obtained from the sum of Curie−Weiss and alternating antiferromagnetic chain

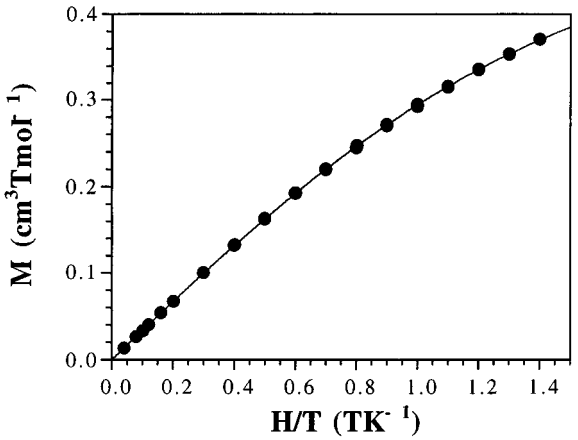

Figure 8. Fitting of the 5 K magnetization of $(BEDT\text{-}TTF)_3[Re_2(NCS)_{10}]\cdot 2CH_2Cl_2$ to the sum of Curie−Weiss and dimer contributions.

contributions. Furthermore the 5 K magnetization isotherm fits closely to the sum of the $S = {}^1/_2$ Curie−Weiss and dimer contributions (see Figure 8).

Together the Curie−Weiss and dimer contributions account for approximately two of the four localized spins, suggesting that the other two spins are paired at high temperature. The most likely situation is that the anion exhibits Curie−Weiss behavior, while B^+ cation couples strongly with a neighboring A^+, leaving one comparatively free A^+ cation per unit cell. Such an assignment suggests that the orientations of B^+ are correlated.

A large single crystal of $(BEDT\text{-}TTF)_2[Re_2(NCS)_{10}]\cdot C_6H_5CN$ (mass ~ 0.5 mg) showed no observable EPR signal at room temperature, suggesting that the cations are spin-paired and that the molecular orbital picture is upheld for the dinegative anion.

Infrared Reflectance. The infrared reflectance spectra of $(BEDT\text{-}TTF)_3[Re_2(NCS)_{10}]\cdot 2CH_2Cl_2$ and $(BEDT\text{-}TTF)_2[Re_2(NCS)_{10}]\cdot C_6H_5CN$ are characteristic of semiconducting behavior, with energy-independent background reflectivities of *ca.* 8 and 11%, respectively. Several vibrational peaks are superimposed on this optical background, the most intense arising from the ν(CN) modes of the anion and the C═C stretching modes from the BEDT-TTF cations. In $(BEDT\text{-}TTF)_2[Re_2(NCS)_{10}]\cdot C_6H_5CN$ additional peaks were detected at 1283 and 1368 cm^{-1}. The vibrational frequencies of the NCS groups confirm the charge assignment of the anions, being in close agreement with a recent solution study[8] (Table 6). Both the terminal and bridging ν(CN) bands shift to lower wavenumber with oxidation, consistent with the behavior expected for σ/π donor ligands. The absence of peaks associated with partial oxidation or reduction (expected to be observable, since the time scale of electronic transfer is longer than that of molecular vibrations) indicates that no significant degree of charge transfer occurs between cation and anion. The angular dependence of the reflectance study gives better distinction between the ν(CN) modes of the terminal $(NCS)^-$ ligands than the solution study, enabling separation of the crystallographically independent modes.

Conclusions

We have investigated the electrocrystallization of BEDT-TTF cations with anions of Re containing N-coordinated thiocyanate ligands. Anions of the form $[Re(NCS)_6]^{2-}$ and $[Re_2(NCS)_8]^{2-}$ do not form characterizable products under these conditions, but two salts containing $[Re_2(NCS)_{10}]^{n-}$ ($n = 2$, 3) have been structurally characterized. Infrared vibrational frequencies unambiguously confirm the different oxidation states of the anion in these salts. There is little change in geometry between the trinegative and dinegative charge states, as might be expected

Table 6. Infrared Vibration Frequencies (cm^{-1}) of Selected Peaks for $(BEDT\text{-}TTF)_3[Re_2(NCS)_{10}]\cdot 2CH_2Cl_2$ and $(BEDT\text{-}TTF)_2[Re_2(NCS)_{10}]\cdot C_6H_5CN$: Comparison with Published Solution Spectra[a]

	C=C modes	bridging $(NCS)^-$	terminal $(NCS)^-$
$(BEDT\text{-}TTF)_3[Re_2(NCS)_{10}]\cdot 2CH_2Cl_2$	1412	1879	2028, 2048, 2063, 2071, 2090
	1419	1917	
$[Re_2(NCS)_{10}]^{3-}$ (in solution)		1885	2058, 2078
		1922	
$(BEDT\text{-}TTF)_2[Re_2(NCS)_{10}]\cdot C_6H_5CN$	1410	1862	2032, 2050, 2073
$[Re_2(NCS)_{10}]^{2-}$ (in solution)		1876	2022, 2062

[a] Reference 8. Note: $N(n\text{-}Bu)_4[PF_6]/CH_2Cl_2$ was the electrolyte for the published solution data.

due to the weak nature of the δ (bonding) and δ^* (antibonding) orbitals.

The two salts of $[Re_2(NCS)_{10}]^{n-}$ ($n = 2, 3$) are unique among BEDT-TTF salts in not containing continuous networks of strongly interacting BEDT-TTF molecules. Nevertheless in both cases there are very short S—S distances between the BEDT-TTF cations and the thiocyanate ligands, thereby potentially allowing a degree of orbital mixing between cation and anion. Both the infrared spectra and the insulating behavior of the two salts suggests that the energy barriers for the processes

$$(BEDT\text{-}TTF)^+ + [Re_2(NCS)_{10}]^{3-} \Leftrightarrow (BEDT\text{-}TTF)^0 + [Re_2(NCS)_{10}]^{2-}$$

$$(BEDT\text{-}TTF)^+ + [Re_2(NCS)_{10}]^{2-} \Leftrightarrow (BEDT\text{-}TTF)^{2+} + [Re_2(NCS)_{10}]^{3-}$$

are large compared to the cation-to-anion electronic transfer integrals. The Hubbard picture is therefore favored for both salts, with a single spin localized on each BEDT-TTF molecule. A small degree of mixing between isolated $(BEDT\text{-}TTF)^+$ may be facilitated by the low-lying anion orbitals, thereby offering a mechanism for magnetic exchange. Susceptibility measurements suggest that there is a considerable degree of magnetic exchange between the $(BEDT\text{-}TTF)^+$ in each structure, although it is not known if cation—anion interactions play a significant role in the exchange pathway.

For both $[Re_2(NCS)_{10}]^{n-}$ salts the activation energy of electrical transport decreases monotonically with decreasing temperature. This behavior is inconsistent with increasing electron mobility, therefore ruling out a delocalized band view of the transport. However, such behavior is closely described by the variable range hopping model, suggesting that electronic tunneling is the primary mechanism of conduction. Despite producing insufficient orbital mixing to lead to delocalization, the low-lying orbitals of the anions may moderate the tunneling energy barrier between the isolated groups of BEDT-TTF. The room temperature conductivities and temperature-dependent activation energies are comparable with many of the semiconducting salts containing continuous networks of strongly interacting BEDT-TTF molecules, suggesting that conduction mechanisms associated with the localized state may occur in these materials also.

Acknowledgment. This work is supported by the U.K. Engineering and Physical Sciences Research Council and the E.U. Human Capital and Mobility Programme. C.J.K. thanks the University of Western Australia for a Hackett Scholarship.

Supporting Information Available: Tables of X-ray crystallographic data, atomic coordinates, site occupation parameters, and anisotropic displacement parameters (21 pages). Ordering information is given on any current masthead page.

IC960884G